# Precise Predictions for Event Shapes in Diphoton Production at the LHC

Federico Buccioni,[1, *] Xuan Chen,[2, †] Wei-Jie Feng,[3, ‡]
Thomas Gehrmann,[3, §] Alexander Huss,[4, ¶] and Matteo Marcoli[5, **]

[1] *Physics Department, Technical University Munich,*
*James-Franck-Strasse 1, 85748 Garching, Germany*
[2] *School of Physics, Shandong University, Jinan, Shandong 250100, China*
[3] *Physik-Institut, Universität Zürich, Winterthurerstrasse 190, 8057 Zürich, Switzerland*
[4] *Theoretical Physics Department, CERN, CH-1211 Geneva 23, Switzerland*
[5] *Institute for Particle Physics Phenomenology, Department of Physics, University of Durham, Durham, DH1 3LE, UK*

Photon pair production is an important benchmark process at the LHC, entering Higgs boson studies and new physics searches. It has been measured to high accuracy, allowing for detailed studies of event shapes in diphoton final states. To enable precision physics with diphoton event shapes, we compute the second-order QCD corrections, $\mathcal{O}(\alpha_s^3)$, to them and study their phenomenological impact.

## INTRODUCTION

The production of photon pairs is a classical hadron collider observable. Following its initial observation at UA2 [1], this process has been measured to increasing accuracy at the Tevatron [2, 3] and the LHC [4, 5]. Photon pair final states played a crucial role in the discovery of the Higgs boson [6, 7] and in subsequent precision studies [8, 9] of the Higgs boson properties. Photon pairs are also widely studied in searches for Physics beyond the Standard Model.

The dominant Standard-Model production process for photon pairs is quark-antiquark annihilation. This Born-level process receives large QCD corrections at next-to-leading order [10] (NLO, $\mathcal{O}(\alpha_s)$) and sizable ones at next-to-next-to-leading order [11–13] (NNLO, $\mathcal{O}(\alpha_s^2)$). The Born-level process enforces the photons to be balanced in transverse momentum. Therefore, the leading-order contribution to the diphoton transverse momentum distribution requires the presence of a partonic recoil in the final state, thus starting only at $\mathcal{O}(\alpha_s)$. The diphoton transverse momentum distribution has also been computed [14] to NNLO QCD, which in this case amounts to $\mathcal{O}(\alpha_s^3)$. Corresponding to a $2 \rightarrow 3$ process at Born level, it is representative of the current frontier in computational complexity in NNLO QCD calculations.

More detailed information on the production dynamics can be gained from the study of event shape distributions in diphoton final states. Event shapes describe geometrical properties of the final-state kinematics [15]. They take non-trivial values at Born level only for final states containing three or more objects. ATLAS have performed a detailed study [4] of diphoton final states at $\sqrt{s} = 13$ TeV, measuring distributions in diphoton transverse momentum and in three event shape variables: hadron collider thrust $a_T$, acoplanarity $\phi_{\text{acop}}$, and decorrelation angle $\phi_\eta^*$. For events at low transverse momentum, scaling relations between the transverse momentum and each of these event shape variables can be estab-

lished [15]. These demonstrate that the event shape distributions are measured with considerably higher resolution than the transverse momentum distribution, mainly owing to the fact that the event shapes rely on the determination of the directions of the photons and not on their energies, which are harder to resolve experimentally.

The event shape distributions are thus ideally suited for high-resolution studies of the QCD dynamics in the production of photon pairs. In the case of the ATLAS measurement [4], a complex interplay between the fiducial selection cuts, applied on the individual photons, and the event shape definition on the photon pair momenta is taking place. These effects can often only be resolved by taking into account higher-order QCD corrections, especially from real radiation and recoils. In this letter, we compute the NNLO QCD corrections, $\mathcal{O}(\alpha_s^3)$, to diphoton event shape distributions and perform detailed studies of their phenomenological impact.

## METHODOLOGY

As for the transverse momentum distribution, non-trivial contributions to the diphoton event shape distributions are generated only in the presence of a partonic recoil. The underlying QCD process is therefore

$$pp \rightarrow \gamma\gamma + \text{jet} + X,$$

with the jet definition replaced by a minimum cut on an event shape variable or on the diphoton transverse momentum. In order to single out direct-photon production and remove hadronic contamination, photons are identified by an isolation criterion defined through a cone around the photon direction. NLO calculations [10] mirror the exact isolation prescription that is used in the experimental measurements. At NNLO, an idealized photon isolation (dynamical cone [16] or hybrid cone [17]) is used.

Renormalized one- and two-loop corrections to the Born process contain explicit infrared (IR) singularities

arising from loop-momentum integration, whereas real-emission matrix elements for the radiation of one or two additional partons exhibit a divergent behavior in soft and collinear configurations. Upon combination of virtual and real corrections, infrared divergences cancel in theoretical predictions for physical observables, but dedicated techniques have to be employed to achieve such cancellation. Our calculation uses the well-established antenna subtraction method [18–20], which extracts the divergent behavior of real-emission corrections locally across phase space by suitable subtraction terms constructed using *antenna functions*. The analytically integrated counterpart of such terms is then used to cancel the explicit singularities of virtual corrections. The numerical integration of infrared-finite remainders is performed within the Monte Carlo event generator NNLO-JET [21].

The six-point one-loop and seven-point tree-level matrix elements for the real-virtual and double-real corrections are obtained from OPENLOOPS2 [22, 23]. The two-loop amplitudes are expressed through their IR-subtracted remainder functions [24]. They have initially been computed in the leading-color approximation [25, 26] (which was used in [14]) and later in full color [27]. The two-loop amplitudes are expressed as linear combinations of massless two-loop five-point integrals [28], which are evaluated in terms of so-called pentagon functions [29]. For the first time, our calculation includes these amplitudes in full color, allowing us to quantify the impact of subleading-color effects.

Due to the large gluon luminosity at the LHC, diphoton cross sections receive sizable contributions from loop-induced gluon-initiated reactions, where the photon pair is radiated off a closed quark loop. The Born level contribution to this process corresponds to the square of a one-loop amplitude, which thus starts contributing only at $\mathcal{O}(\alpha_s^3)$, as part of the full NNLO contribution. Owing to this delayed perturbative onset, the loop-induced gluon fusion contribution has been identified to be responsible for a substantial fraction of the scale uncertainty in diphoton-plus-jet cross sections at NNLO [14]. Higher-order corrections to this process, originally studied in [30] for the gluon-initiated channels only, are formally beyond NNLO accuracy, but they can reduce the theoretical uncertainty. In this letter, we assess the impact of the complete NLO, $\mathcal{O}(\alpha_s^4)$, correction to this loop-induced process, including all its partonic initial states. The virtual corrections to this process are given by the interference of five-point one- and two-loop amplitudes. The full-color two-loop contributions of the $gg \to \gamma\gamma g$ process were presented in [31] and are distributed through the NJET library [32]. The analogous amplitudes for the $q\bar{q} \to \gamma\gamma g$ process, and crossings thereof, were computed in [27]. Real-radiation corrections, which entail six-point one-loop squared amplitudes, are obtained from OPEN-LOOPS2 in all partonic channels.

The NNLOJET implementation was validated in various ways. For the real corrections, the numerical evaluation of antenna subtraction terms was tested pointwise against OPENLOOPS2 matrix elements in each IR-singular phase-space region. For the virtual ones, we checked that the universal IR-pole structure of one- and two-loop amplitudes [24] is reproduced by the integrated antenna functions. At cross-section level, we compared our results for diphoton plus one and two jets at NLO accuracy against `MadGraph5_aMC@NLO` [33, 34], finding agreement. Finally, at NNLO we reproduce the diphoton-plus-jet differential cross sections of [14], by truncating the two-loop virtual corrections to leading-color for consistency.

## RESULTS

The ATLAS 13 TeV analysis [4] of diphoton event shapes is performed in the fiducial region defined by the following cuts:

$$p_{T,\gamma_1} > 40 \text{ GeV}, \quad p_{T,\gamma_2} > 30 \text{ GeV},$$
$$|\eta_\gamma| \in (0, 1.37) \cup (1.52, 2.37), \quad \Delta R_{\gamma\gamma} > 0.4.$$

The photons are identified by a fixed-cone isolation criterion, allowing a maximum hadronic energy fraction $\epsilon_{T,\gamma}$ inside a cone of radius $R$ around the photon direction, with $(R, \epsilon_{T,\gamma}) = (0.2, 0.09)$. We note that this $R$ value is at the lower end of what is typically used in single-photon measurements [35].

In our theoretical prediction we use the PDF set `PDF4LHC21_mc` [36] and we adopt a hybrid-cone isolation prescription [17] which inserts a dynamical cone [16] of parameters $(R_d, \epsilon_d, n) = (0.1, 0.15, 1)$ inside the fixed isolation cone. The renormalization and factorization scales are chosen dynamically using the central scale $\mu_0^2 = E_{T,\gamma\gamma}^2 = m_{\gamma\gamma}^2 + p_{T,\gamma\gamma}^2$. Theoretical uncertainties are estimated via 7-point scale variations, namely by varying $\mu_R$ and $\mu_F$ with multiplicative factors $\xi_{R,F} \in [1/2, 2]$ imposing $1/2 \leqslant \mu_R/\mu_F \leqslant 2$.

In total, the ATLAS measurement presents one-dimensional distributions in eight different diphoton variables. Four of these distributions, $p_{T,\gamma_1}$, $p_{T,\gamma_2}$, $m_{\gamma\gamma}$, and $|\cos\theta^*|_{\text{CS}}$, receive Born-level contributions already at $\mathcal{O}(\alpha_s^0)$. They are compared to NNLO QCD predictions [13] from NNLOJET already in [4]. The four remaining distributions start only at $\mathcal{O}(\alpha_s)$: transverse momentum of the diphoton system $p_{T,\gamma\gamma}$ and the three event shapes [15]:

$$a_T = 2 \cdot \frac{|p_{x,\gamma_1}p_{y,\gamma_2} - p_{y,\gamma_1}p_{x,\gamma_2}|}{|\vec{p}_{T,\gamma_1} - \vec{p}_{T,\gamma_2}|}, \quad (1)$$

$$\phi_\eta^* = \tan\frac{\pi - \Delta\phi_{\gamma\gamma}}{2}\sqrt{1 - \tanh^2(\Delta\eta_{\gamma\gamma}/2)}, \quad (2)$$

$$\phi_{\text{acop}} = \pi - \Delta\phi_{\gamma\gamma}. \quad (3)$$

| Observable | Cut | Equivalent $p_{T,\gamma\gamma}$ [GeV] |
|---|---|---|
| $p_{T,\gamma\gamma}$ [GeV] | 1.0 | – |
| $a_T$ [GeV] | 1.08 | 1.52 |
| $\phi_\eta^*$ | 0.0105 | 1.19 |
| $\phi_{\rm acop}$ | 0.0234 | 1.12 |

TABLE I. Lower cuts on the event shapes applied in our comparison to the ATLAS data [4] and their conversion to an equivalent value of $p_{T,\gamma\gamma}$, assuming $m_{\gamma\gamma} = 80$ GeV.

Our NNLO QCD calculation enables accurate predictions for these four observables, and in the following we exclusively focus on them.

At the lower endpoint of event shape distributions, the fixed-order description breaks down due to the emergence of large logarithmic corrections at each order in perturbation theory that need to be resummed for reliable predictions. Also, in these endpoint regions the numerical evaluation of the fixed-order components becomes increasingly challenging. We therefore cut off the distributions at bin edges in the respective measurement, listed in Table I. At the event-generation level, an event is accepted if it passes at least one of these cuts, which ensures the infrared-safety of the evaluation.

Towards lower values of transverse momentum or event shapes, the final-state photons approach a back-to-back configuration, leading to a diphoton-invariant mass of $m_{\gamma\gamma} \geqslant 80$ GeV, corresponding to twice the cut on $p_{T,\gamma_1}$. In these back-to-back configurations, the cutoff values in Table I are related by the approximate scaling [15, 37]:

$$p_{T,\gamma\gamma} \approx \sqrt{2} a_T,$$
$$p_{T,\gamma\gamma}/m_{\gamma\gamma} \approx \sqrt{2}\phi_\eta^* \approx 0.85\sqrt{2}\tan(\phi_{\rm acop}/2). \quad (4)$$

Figure 1 presents the theoretical prediction up to NNLO in comparison to the ATLAS data [4]. Overall, we observe that the inclusion of NNLO corrections leads to an improved description of the data in the region where the transverse momentum or the values of the event shape variables are sufficiently large. In these regions, the NNLO corrections are positive and the scale uncertainty on the theory predictions typically drops from around $\pm(10\ldots15)\%$ at NLO to $\pm(2\ldots10)\%$ at NNLO. Although the NNLO corrections bring the NLO curve closer to the data in these regions, the theory predictions still fall systematically below the measurements.

Towards the lower end of all distributions (below $p_{T,\gamma\gamma} \approx 10$ GeV and equivalent values of the shape variables), the NLO and NNLO predictions are systematically above the experimental data. NNLO corrections are still moderate in the kinematical range displayed in Figure 1, and an apparent perturbative convergence is observed in this range, with NNLO predictions typically within the NLO scale uncertainty, even if here one expects all-order resummation to be needed for reliable predictions. We observe in particular that the bin resolution in this region is considerably higher for $a_T$, $\phi_\eta^*$ and $\phi_{\rm acop}$ than it is for $p_{T,\gamma\gamma}$. This superior resolution allows to probe this infrared-sensitive region considerably more accurately than through the $p_{T,\gamma\gamma}$ spectrum.

Above $p_{T,\gamma\gamma} \approx 70$ GeV, we observe a bump in the transverse momentum distribution, which is a consequence of the the fiducial cuts that are applied in the measurement. No explicit cut is imposed on the diphoton-invariant mass, which is only implicitly restricted from below through the photon angular separation $\Delta R_{\gamma\gamma} > 0.4$. Low invariant-mass photon pairs require both photons to be in the same hemisphere, such that their combined transverse momentum must be balanced by a partonic recoil. Consequently, these low-mass photon pairs contribute to the transverse momentum distribution only above $p_{T,\gamma\gamma} \sim 70$ GeV, corresponding to the sum of the individual $p_{T,\gamma}$ cuts. Similar features, though less pronounced, are observed in all event shape distributions. Also, they are stable under perturbative corrections, indicating that they do not give rise to large logarithms.

The NLO, $\mathcal{O}(\alpha_s^4)$, correction to the process where both photons couple to a closed quark loop is added to the NNLO, $\mathcal{O}(\alpha_s^3)$, predictions to yield the yellow NNLO$^+$ curves in Figure 1. At large values of event shapes and $p_{T,\gamma\gamma}$, the inclusion of this contribution does not reduce the NNLO scale uncertainty in a visible manner, contrary to initial expectations [14, 30]. For medium and low values of event shapes and transverse momentum, the NLO corrections to this subprocess become large and negative, leading to a substantial deterioration of the perturbative convergence of the NNLO$^+$ predictions.

Compared to previous NNLO results for diphoton final states at finite transverse momentum [14], we now take into account the complete color information at two-loop level. The newly included subleading color terms receive contributions from non-planar two-loop five-point amplitudes, which are also present in the the gluon-induced quark-loop subprocess at order $\alpha_s^4$. We quantify the numerical impact of these newly included terms in Figure 2, which displays the $p_{T,\gamma\gamma}$, $a_T$, $\phi_\eta^*$ and $\phi_{\rm acop}$ distributions, comparing the full NNLO with the results obtained by neglecting or including specific contributions.

The impact of the finite remainder of the two-loop virtual corrections is indicated in the upper frames of Figure 2. More specifically, we isolate the interference of the two-loop amplitude with the tree-level one $(2{\rm Re}(A_0 \cdot A_2^*))$ and we either remove it completely (label 'no VV') or we include only its leading-color component (label 'LC VV'). In terms of two-loop Feynman diagrams, the leading-color component is defined as in [14]. However, we note that our definition of finite remainder [24, 27] differs from the one of [14, 26]. It can be seen that the contribution of the complete two-loop finite remainder depends non-trivially on the kinematics. It is quasi negligible for large
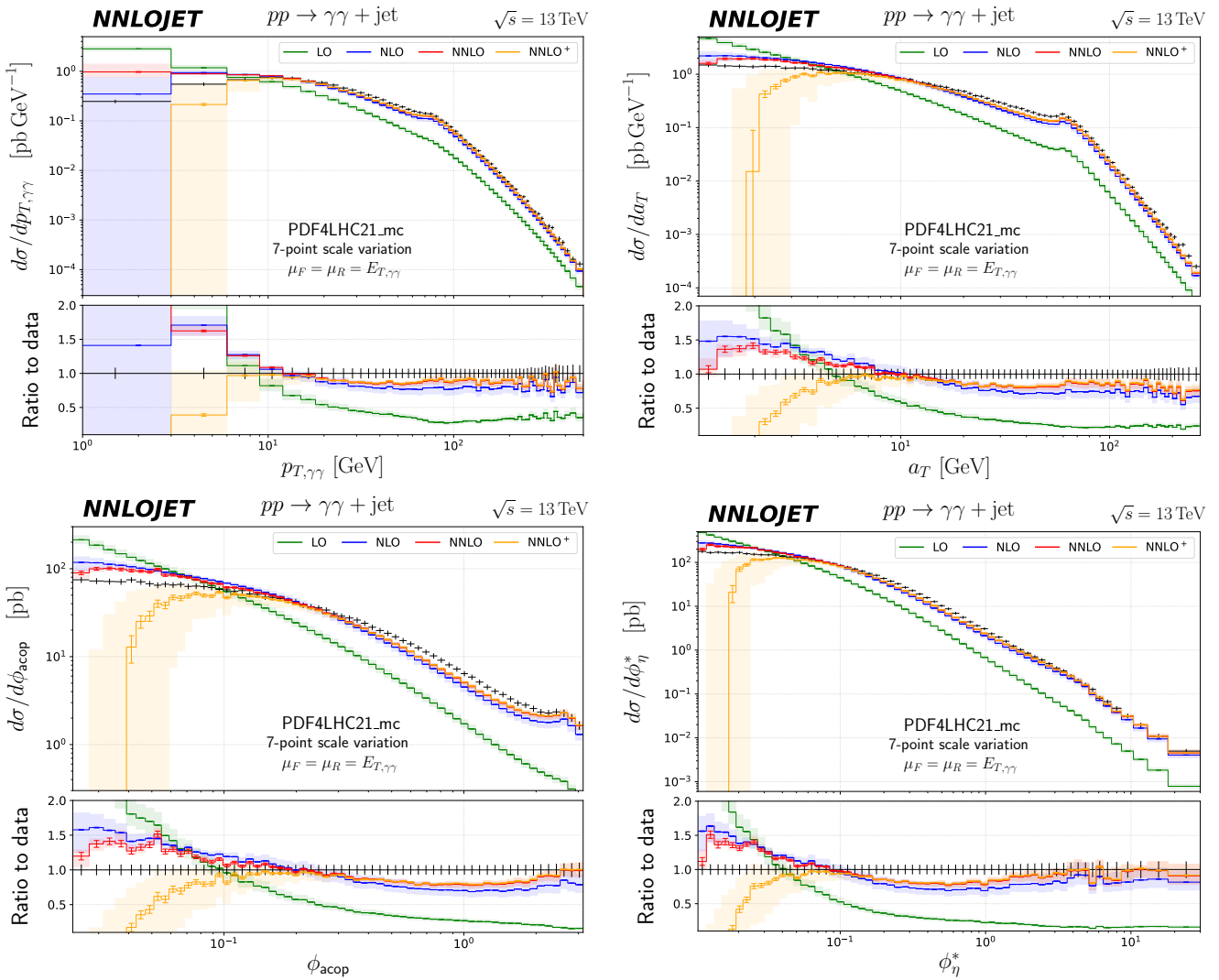
FIG. 1. $p_{T,\gamma\gamma}$, $a_T$, $\phi_{\mathrm{acop}}$ and $\phi_\eta^*$ distributions for diphoton production at the LHC in LO (green), NLO (blue) and NNLO (red) accuracy, in comparison with the ATLAS diphoton measurement [4]. The NNLO prediction consistently includes the loop-induced gluon-initiated process at Born level. The NNLO$^+$ curve (yellow) is obtained by including the $\mathcal{O}(\alpha_s^4)$ NLO correction to the loop-induced process. The colored bands represent theoretical uncertainties from 7-point scale variation. The error bars represent Monte-Carlo integration errors. The ratio plots show the prediction normalized to the ATLAS data.

values of the event shapes or $p_{T,\gamma\gamma}$, and typically amounts to less than 5% of the NNLO prediction except at the low endpoints of the distributions. This is largely dominated by the leading-color component, with subleading color terms never exceeding the 0.3% level.

In the lower frame of Figure 2, we study the impact of the gluon-induced quark-loop subprocess, which is by default included at order $\alpha_s^3$ in the NNLO predictions. Its numerical relevance can be seen from the 'no QL', where this subprocess is removed entirely. In the NNLO$^+$ curves, the $\mathcal{O}(\alpha_s^4)$ corrections to this subprocess are included. It can be seen that the quark-loop subprocess contributes in particular in the low and intermediate range in the distributions. Its inclusion at NNLO is crucial for the perturbative stability of the predictions at

this order, especially towards the lower end of the distributions. This feature is remarkable, since at NNLO this contribution appears for the first time, being finite and unrelated to any of the other subprocesses. The $\mathcal{O}(\alpha_s^4)$ corrections to the quark-loop subprocesses, included in NNLO$^+$, are very small in the bulk of the distributions, and become very sizable and negative only towards their lower ends. Their smallness in the bulk explains their negligible impact on the scale uncertainty, where a small improvement is observed only in the medium range of the distributions. This effect quickly deteriorates at lower values.
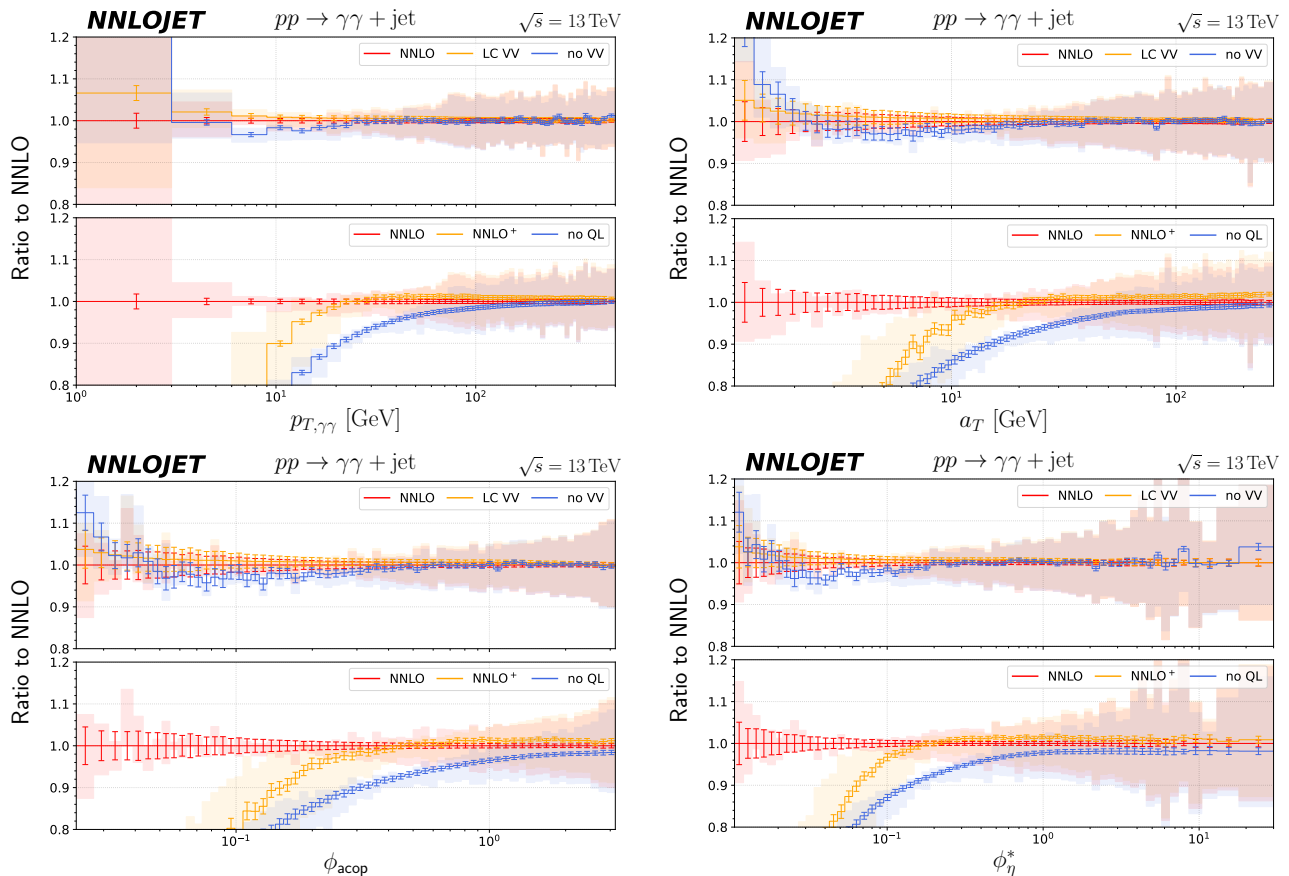
FIG. 2. Numerical impact of virtual two-loop corrections (upper frames): comparison of the full calculation at NNLO (red, 'NNLO'), calculation without the two-loop finite reminder $2\mathrm{Re}\,(A_0 \cdot A_2^*)$ (blue, 'no VV') and calculation obtained including only the leading-color contribution to the two-loop finite reminder (yellow, 'LC VV'). Numerical impact of loop-induced processes (lower frames): comparison of the full calculation at NNLO (red, 'NNLO'), calculation without the gluon-initiated $\mathcal{O}(\alpha_s^3)$ quark-loop contribution (yellow, 'no QL') and calculation obtained including it and the $\mathcal{O}(\alpha_s^4)$ NLO correction (orange, 'NNLO$^+$').

## CONCLUSIONS

In this letter, we computed the NNLO QCD corrections to the diphoton transverse momentum distribution and to event shape distributions related to it. The corrections considerably improve the description of AT-LAS data [4] for these precision observables. The distributions display several kinematical features, which can be explained through an intricate interplay between the diphoton observables definition and the fiducial cuts on the individual photons. We quantified the numerical impact of previously unaccounted contributions from process classes containing two-loop non-planar virtual corrections, supporting the validity of leading-color truncations for generic two-loop amplitudes. We investigated the impact of quark-loop induced subprocesses, demonstrating their relevance at low and intermediate values of the shape variables at NNLO, and highlighting the need for their consistent inclusion at order $\alpha_s^3$.

Our results will enable precision phenomenology studies with event shape distributions in diphoton final states.

By demonstrating the numerical convergence and stability of the NNLO predictions at low values of transverse momentum, they also represent an important step towards the third-order QCD corrections for more inclusive diphoton observables.

* federico.buccioni@tum.de
† xuan.chen@sdu.edu.cn

‡ weijie.feng@physik.uzh.ch
§ thomas.gehrmann@uzh.ch
¶ alexander.huss@cern.ch
** matteo.marcoli@durham.ac.uk

[1] J. Alitti *et al.* (UA2), Phys. Lett. B **288**, 386 (1992).
[2] T. Aaltonen *et al.* (CDF), Phys. Rev. Lett. **110**, 101801 (2013), arXiv:1212.4204 [hep-ex].
[3] V. M. Abazov *et al.* (D0), Phys. Lett. B **725**, 6 (2013), arXiv:1301.4536 [hep-ex].
[4] G. Aad *et al.* (ATLAS), JHEP **11**, 169 (2021), arXiv:2107.09330 [hep-ex].
[5] S. Chatrchyan *et al.* (CMS), Eur. Phys. J. C **74**, 3129 (2014), arXiv:1405.7225 [hep-ex].
[6] G. Aad *et al.* (ATLAS), Phys. Lett. B **716**, 1 (2012), arXiv:1207.7214 [hep-ex].
[7] S. Chatrchyan *et al.* (CMS), Phys. Lett. B **716**, 30 (2012), arXiv:1207.7235 [hep-ex].
[8] G. Aad *et al.* (ATLAS), JHEP **08**, 027 (2022), arXiv:2202.00487 [hep-ex].
[9] A. Tumasyan *et al.* (CMS), JHEP **07**, 091 (2023), arXiv:2208.12279 [hep-ex].
[10] T. Binoth, J. P. Guillet, E. Pilon, and M. Werlen, Eur. Phys. J. C **16**, 311 (2000), arXiv:hep-ph/9911340.
[11] S. Catani, L. Cieri, D. de Florian, G. Ferrera, and M. Grazzini, Phys. Rev. Lett. **108**, 072001 (2012), [Erratum: Phys.Rev.Lett. 117, 089901 (2016)], arXiv:1110.2375 [hep-ph].
[12] J. M. Campbell, R. K. Ellis, Y. Li, and C. Williams, JHEP **07**, 148 (2016), arXiv:1603.02663 [hep-ph].
[13] T. Gehrmann, N. Glover, A. Huss, and J. Whitehead, JHEP **01**, 108 (2021), arXiv:2009.11310 [hep-ph].
[14] H. A. Chawdhry, M. Czakon, A. Mitov, and R. Poncelet, JHEP **09**, 093 (2021), arXiv:2105.06940 [hep-ph].
[15] A. Banfi, S. Redford, M. Vesterinen, P. Waller, and T. R. Wyatt, Eur. Phys. J. C **71**, 1600 (2011), arXiv:1009.1580 [hep-ex].
[16] S. Frixione, Phys. Lett. B **429**, 369 (1998), arXiv:hep-ph/9801442.
[17] F. Siegert, J. Phys. G **44**, 044007 (2017), arXiv:1611.07226 [hep-ph].
[18] A. Gehrmann-De Ridder, T. Gehrmann, and E. W. N. Glover, JHEP **09**, 056 (2005), arXiv:hep-ph/0505111.
[19] A. Daleo, T. Gehrmann, and D. Maitre, JHEP **04**, 016 (2007), arXiv:hep-ph/0612257.
[20] J. Currie, E. W. N. Glover, and S. Wells, JHEP **04**, 066 (2013), arXiv:1301.4693 [hep-ph].
[21] A. Gehrmann-De Ridder, T. Gehrmann, E. W. N. Glover, A. Huss, and T. A. Morgan, Phys. Rev. Lett. **117**, 022001 (2016), arXiv:1507.02850 [hep-ph].
[22] F. Cascioli, P. Maierhofer, and S. Pozzorini, Phys. Rev. Lett. **108**, 111601 (2012), arXiv:1111.5206 [hep-ph].
[23] F. Buccioni, J.-N. Lang, J. M. Lindert, P. Maierhöfer, S. Pozzorini, H. Zhang, and M. F. Zoller, Eur. Phys. J. C **79**, 866 (2019), arXiv:1907.13071 [hep-ph].
[24] S. Catani, Phys. Lett. B **427**, 161 (1998), arXiv:hep-ph/9802439.
[25] B. Agarwal, F. Buccioni, A. von Manteuffel, and L. Tancredi, JHEP **04**, 201 (2021), arXiv:2102.01820 [hep-ph].
[26] H. A. Chawdhry, M. Czakon, A. Mitov, and R. Poncelet, JHEP **07**, 164 (2021), arXiv:2103.04319 [hep-ph].
[27] B. Agarwal, F. Buccioni, A. von Manteuffel, and L. Tancredi, Phys. Rev. Lett. **127**, 262001 (2021), arXiv:2105.04585 [hep-ph].
[28] D. Chicherin, T. Gehrmann, J. M. Henn, P. Wasser, Y. Zhang, and S. Zoia, Phys. Rev. Lett. **123**, 041603 (2019), arXiv:1812.11160 [hep-ph].
[29] D. Chicherin and V. Sotnikov, JHEP **20**, 167 (2020), arXiv:2009.07803 [hep-ph].
[30] S. Badger, T. Gehrmann, M. Marcoli, and R. Moodie, Phys. Lett. B **824**, 136802 (2022), arXiv:2109.12003 [hep-ph].
[31] S. Badger, C. Brønnum-Hansen, D. Chicherin, T. Gehrmann, H. B. Hartanto, J. Henn, M. Marcoli, R. Moodie, T. Peraro, and S. Zoia, JHEP **11**, 083 (2021), arXiv:2106.08664 [hep-ph].
[32] S. Badger, B. Biedermann, P. Uwer, and V. Yundin, Comput. Phys. Commun. **184**, 1981 (2013), arXiv:1209.0100 [hep-ph].
[33] J. Alwall, R. Frederix, S. Frixione, V. Hirschi, F. Maltoni, O. Mattelaer, H. S. Shao, T. Stelzer, P. Torrielli, and M. Zaro, JHEP **07**, 079 (2014), arXiv:1405.0301 [hep-ph].
[34] R. Frederix, S. Frixione, V. Hirschi, D. Pagani, H. S. Shao, and M. Zaro, JHEP **07**, 185 (2018), [Erratum: JHEP 11, 085 (2021)], arXiv:1804.10017 [hep-ph].
[35] G. Aad *et al.* (ATLAS), JHEP **07**, 086 (2023), arXiv:2302.00510 [hep-ex].
[36] R. D. Ball *et al.* (PDF4LHC Working Group), J. Phys. G **49**, 080501 (2022), arXiv:2203.05506 [hep-ph].
[37] A. Gehrmann-De Ridder, T. Gehrmann, E. W. N. Glover, A. Huss, and T. A. Morgan, JHEP **11**, 094 (2016), [Erratum: JHEP 10, 126 (2018)], arXiv:1610.01843 [hep-ph].